JOURNAL OF GEOPHYSICAL RESEARCH, VOL. 89, NO. A8, PAGES 6599–6612, AUGUST 1, 1984

Helios Observational Constraints on Solar Wind Expansion

E. MARSCH AND A. K. RICHTER

Max-Planck-Institut für Aeronomie, Katlenburg-Lindau, Federal Republic of Germany

Helios particle and magnetic field observations between 0.3 and 1 AU are used to determine plasma parameters that characterize the bulk and internal energy state of the solar wind. Quantities expected to be conserved in a time-stationary flow with local spherical symmetry in the ecliptic plane are actually found to be invariant within measurement uncertainties. These are the total mass, energy, and angular momentum fluxes for the anisotropic solar wind plasma composited by electrons, protons, and alphas. Although individual species have nonthermal velocity distributions, the total plasma pressure is almost isotropic ($p_\perp/p_\parallel = 0.9$). The total heat flux divided by the mass flux $Q_r/\rho u_r$ is markedly smaller than thermal speeds squared $v_{\parallel,\perp}{}^2 = p_{\parallel,\perp}/\rho$. By this reason an appropriately defined polytropic index γ is found to be almost $\frac{4}{3}$ and rather insensitive to heliocentric distance and flow speed. This index γ does not include terms due to wave turbulence or external heat sources but is solely based on the total particle heat flux. These observational findings indicate that the heat flux beyond 0.3 AU is observationally too small to cause a strong departure from adiabaticity. The solar wind expansion may be conceived in terms of a "single particle" moving in the binding gravitational potential and in the accelerating thermal (enthalpy and heat fluxes) and magnetorotational (azimuthal kinetic energy and Poynting flux) potentials. The radial profiles of these potentials are derived from observations.

1. INTRODUCTION

The Helios solar probes provide the unique opportunity to study radial variations of solar wind plasma parameters in the inner heliosphere, since their highly elliptical orbits about the sun cover the heliocentric distance range between 0.3 and 1 AU. Detailed Helios in situ particle observations by *Rosenbauer et al.* [1977], *Marsch et al.* [1982*a*, *b*], *Pilipp et al.* [1981], and *Schwenn* [1983] yield experimental constraints on modeling the radial evolution of distribution functions and, by taking velocity moments, observational constraints on theoretical fluid models for the wind expansion. In many papers of various authors [*Parker*, 1963: *Meyer and Pfirsch*, 1968; *Weber and Davis*, 1970; *Holzer and Axford* 1970; *Weber*, 1970; *Hollweg*, 1973; *Barnes*, 1974; *Acuna and Whang*, 1976] a fairly general theoretical framework, based on the pioneering paper by *Weber and Davis* [1967], has been advanced by taking the multicomponent (electrons and protons) and anisotropic nature of the plasma and the inhomogeneity of the interplanetary medium into account, as well as the angular momentum transport in the solar wind. In addition, we shall also include the alpha particles, since Helios observations indicate that they should not be treated as a minor species. The generalization of the model equations is obvious and outlined in the appendix. Within this theory we shall discuss various physical quantities that can be estimated from the observations and that are regarded to be basic from a theoretical point of view, as, for example, the fluxes of the total mass, angular momentum, and energy.

The purpose of the present paper is to consider these physical quantities and others detailed below in order to derive more stringent constraints for any solar wind model. We also like to assess briefly the possibility whether a thermally driven solar wind model appears feasible considering in particular the Helios perihelion (0.3 AU) observations. This question is of importance since with the detection of the electron strahl [*Rosenbauer et al.*, 1976; *Pilipp*, 1983] the possibility of a wind driven by these suprathermal, exospheric-type electrons has emerged and recently been discussed by *Olbert* [1981]. Furthermore, the importance of the alpha particles in correctly evaluating the bulk properties, such as the ion mass flux or the angular momentum [*Pizzo et al.*, 1983] carried by the solar wind, has been emphasized by Helios observations. Among these is the finding that alphas move faster than protons by a considerable fraction of the local Alfvén speed [*Asbridge et al.*, 1976; *Marsch et al.*, 1982*b*] and thus at times can contribute essentially to the solar wind internal energy. These observations call for a multifluid approach in modeling the expansion and necessitate that alphas be regarded as a major constituent of the solar wind plasma.

In the above references and more recently, for example, in the papers by *Holzer and Leer* [1980] and *Leer et al.* [1982], the physical invariants and conserved quantities expected from a model with local spherical symmetry restricted to the ecliptic plane have been extensively discussed. All physical parameters were assumed to vary only with heliocentric distance. The theory yields two groups of parameters that are related to bulk properties of the wind and to the internal energy, respectively, comprising contributions from protons, alphas, and electrons. The outline of this paper is the following: We start with some general remarks on the Helios data. Concerning the definition of relevant parameters we refer to the appendix or otherwise give explicit expressions. We then discuss the variations of bulk properties with radial distance from the sun. In the subsequent section we investigate the radial evolution of internal energy and total heat flux with emphasis on an appropriately defined polytropic index γ that allows to evaluate the data in usual thermodynamic terms and to compare with the situation where an equation of state exists. Then we shall concentrate on the radial evolution of the kinetic energy per amu and of some effective potentials that we define later on. These potentials involve heat and enthalpy fluxes and the magnetic field effects due to the sun's rotation. The expansion of the wind can transparently be described as the motion of a "single particle" moving in these potentials and in the sun's binding gravitational potential. Our paper will conclude with a summary and a section discussing the relevance of our observational constraints on solar wind modeling.

Copyright 1984 by the American Geophysical Union.

Paper number 4A0591.
0148-0227/84/004A-0591$05.00

2. HELIOS OBSERVATIONS

2.1. *General Remarks*

In this section we shall discuss the plasma measurements obtained by the Helios 1 and 2 spacecraft between 0.3 and 1 AU. The plasma instruments and data analysis have extensively been described by *Schwenn et al.* [1975], *Rosenbauer et al.* [1977], *Marsch et al.* [1982*a*, *b*], *Pilipp et al.* [1981], and *Pillipp* [1983]. The magnetic field data have been provided by the magnetometer team of the University of Braunschweig. Details can be found in the work of *Neubauer et al.* [1977*a*, *b*] and *Musmann et al.* [1977]. The "average" solar wind in the inner heliosphere (structures and slow variations) has been investigated on a statistical basis by *Schwenn* [1983]. In order to put these Helios plasma parameters into the context of previously measured particle distributions and solar wind data, the reader is advised to compare with *Feldman et al.* [1975, 1976, 1977]. The papers by *Neugebauer* [1981, 1983] review helium ion observations and present experimental constraints on solar wind acceleration mechanisms. A description of the various types of solar wind flow and their relation to solar activity is also given by *Hundhausen* [1979].

Before embarking on a discussion of the actual data, we shall briefly outline the idea of our analysis and discuss some relevant points. The helios plasma analyzer provides combined three-dimensional ion velocity distributions, in which the most abundant hydrogen and helium ions still have to be separated. Details of the applied separation procedure required for the Helios E/q measuring instruments can be found in the articles by *Rosenbauer et al.* [1977] and *Marsch et al.* [1982*a*, *b*]. The electron analyzer integrates the incident flux over an elevation angle of about $\pm 10°$ with respect to the ecliptic plane. Exploiting the assumption of gyrotropy, the measured two-dimensional electron distributions can be extended to the third dimension of velocity space. In order to minimize the possible error introduced in the electron data by this procedure we restrict the data set to those spectra where the magnetic field vector is within $\pm 5°$ in the ecliptic plane. This restriction guarantees that the so-called strahl [*Rosenbauer et al.*, 1976] is completely measured by the electron analyzer. Since the strahl electrons constitute a major part of the total heat flux, the above condition appears mandatory for our data evaluation.

The particle parameters required for our analysis are the velocity moments. We need the density n_j, flow speed $\mathbf{v}_j$, temperatures $T_{j\parallel}$ and $T_{j\perp}$, and intrinsic heat fluxes $q_{j\parallel}$ and $q_{j\perp}$ for the various species j. Single fluid quantities such as the total particle mass density, the bulk flow velocity $\mathbf{u}$, the total pressure $\mathbf{P}$, and the heat flux $\mathbf{Q}$ can then be calculated according to (A1), (A8), (A12), and (A13), given in the appendix. Finally, these quantities have to be transformed from the spacecraft frame into the standard heliocentric coordinate system in order to compare with the model equations.

All figures in this paper are based on the Helios primary missions, comprising the time interval from day 344 in 1974 to day 95 in 1975 (Helios 1) and the time interval from day 17 to 130 in 1976 (Helios 2). These time periods belong to the phase about minimum solar activity. They are characterized by recurrent, sharply bounded high-velocity streams [*Schwenn et al.*, 1978] originating from coronal holes [*Hundhausen*, 1979] separated by low-speed, cold, and dense solar wind flows, in which the heliospheric current sheet is embedded [*Marsch et al.*, 1982*a*, *b*; *Behannon et al.*, 1981]. In order to account for this two-state phenomenon of the solar wind we have classified the data into three classes corresponding to low- (200–400), intermediate- (400–600), and high-speed (600–800 km s^{-1}) flow. In order to derive average radial gradients of all solar wind parameters, we additionally have sorted the data into radial distance bins of 0.1 AU in width. The mean values of the respective parameters have been plotted as well as their corresponding standard deviations. Since we are interested in the large-scale evolution of the solar wind, we used 10-min averages over individual spectra (sampling time of 40.5 s) as quasi-spectra for our statistical analysis. The reason was that we often encountered the situation that in one cycle we had reliable data only for a single particle species, say, electrons, whereas for the subsequent spectrum only proton data were available. By this technique our data base has been enlarged to about 8300 quasi-spectra.

2.2. *The Constants of Motion*

This section is devoted to investigate the global constants of motion $\dot{M}$, L, ε, and F_B, being the mass flux, the specific angular momentum, the total energy per proton mass, and the magnetic flux, respectively. All these quantities are defined in detail in the appendix. The relevance of these constants of motion for the description of a spherically symmetric solar wind expansion in the ecliptic plane has been discussed by many authors (see the introduction). For further references see also the more recent review by *Leer et al.* [1982].

First, we shall consider the angular momentum L. This quantity has already been analyzed before by *Pizzo et al.* [1983]. These authors thoroughly discussed the problem of determining the sun's angular momentum loss and addressed extensively the root of the observational problem on how to assess correctly such an elusive quantity as the azimuthal flow speed of the solar wind. We do not want to repeat their discussion and simply refer to the above paper also in view of other important details, such as the instrument calibration and corrections that have to be applied to the raw data. However, it is necessary to emphasize the following point: The real solar wind being structured in recurrent high- and low-speed streams severely violates the theoretical assumption of local spherical symmetry. Since our model deals with the unstructured ideal high- or low-speed wind, we cannot expect to predict correctly radial trends for quantities such as the angular momentum that are highly sensitive to possible azimuthal variations in the magnetic field and flow velocity components. The reader should keep this in mind when we later present the trend analysis of L, $\dot{M}L$, and u_ϕ. Stream-stream interactions, for example, can entirely mask the "true" evolution of the angular momentum carried away from the sun by the undisturbed wind.

Along the same line of arguments we have ignored spectra associated with smaller time scale structures such as shocks and discontinuities, noncompressive density enhancements [*Gosling et al.*, 1978], and helium-rich events [*Borrini et al.*, 1980]. Nevertheless, our data that are contained either in the velocity bin below 400 km s^{-1} or in the class from 400 to 600 km s^{-1} corresponding to stream interaction zones still represent a mixture of plasma parcels that are probably not comparable. The ideal situation would be to rely solely on data sets from radial lineup constellations of the twin Helios probes. One good lineup in a typical high-speed stream has been discussed in detail by *Schwartz and Marsch* [1983]. Unfortunately, the data base from Helios lineups is too sparse for the present investigation. Therefore we shall bin the data ac-

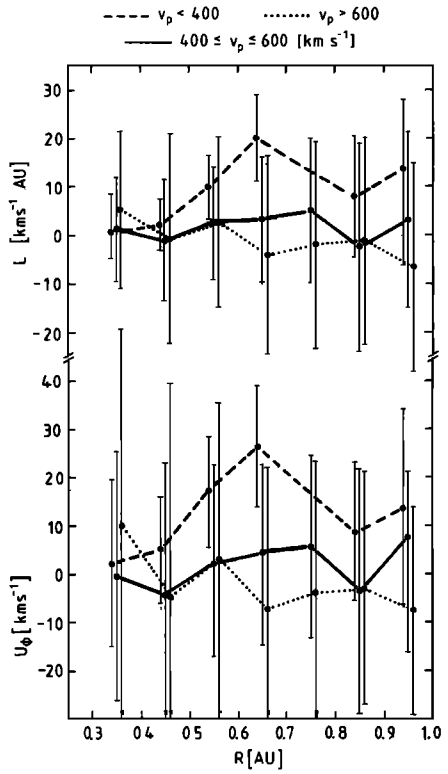

Fig. 1. Specific angular momentum (top) and azimuthal component of the bulk velocity (bottom) versus heliocentric distance in AU. Error bars give the standard deviation of the mean for each radial distance bin with a width of 0.1 AU. The curves correspond to high-speed (dotted curve), intermediate-speed, (solid curve) and low-speed (dashed curve) solar wind.

cording to speed and heliocentric distance irrespective of whether these data were sampled within identical flux tubes or not.

Figure 1 (bottom part) shows the azimuthal bulk flow velocity component u_ϕ (protons and alphas) in kilometers per second for the three velocity classes—slow ($\lesssim$400 km s^{-1}, dashed curve), intermediate (400–600 km s^{-1}, solid curve), and fast solar wind ($\gtrsim$600 km s^{-1}, dotted curve)—as a function of heliocentric radial distance. Each point represents an average over a distance bin of 0.1 AU in width. The error bars have been slightly displaced from one another in order to avoid overlapping. Note the large variances in the data, which are due to intrinsic measurement errors for u_ϕ and due to real variations caused by stream-stream interactions, waves, time variability, etc. Therefore, individual values should not be directly compared with theoretical predictions given by *Weber and Davis* [1967]. Numerical values and standard deviations are given in Table 1.

The azimuthal velocity component is one of the two terms that compose the specific angular momentum L according to (A9). This explains the similarity of the top and bottom lines in Figure 1, which also displays L in the same format as u_ϕ. Note that the angular momentum per amu is given in AU km s^{-1}. As for u_ϕ, there is a distinct trend for L to be negative, against the sense of corotation with the sun, in fast solar wind and to be positive in slow solar wind. This trend has been found by *Pizzo et al.* [1983], and it has been explained in terms of stream interaction dynamics that may lead to a deflection of the dilute high-speed gas at the dense slow plasma. By averaging over radial distance and speed bins one finds $L = (1.7 \pm 19)$ AU km s^{-1}. This locates the Alfvén critical radius in units of the solar radius at $r_A/R_S = [L/(\Omega R_S{}^2)]^{1/2} \approx 13$, a figure already quoted by *Pizzo et al.* [1983]. It should be noted, however, that L bears a very large error and is most severly affected by measurement uncertainties. Strictly speaking, the fact that real solar wind is highly structured makes a straightforward application of the Weber and Davis model (hereafter referred to as WD model) questionable. For example, negative values for L and u_ϕ are not compatible with an initially partly corotating plasma that is progressively accelerated through the Alfvénic point and decoupled from the sun. Thus negative L can only result from interplanetary dynamical processes. However, if one takes the larger L value (see Table 1) in the slow wind, $L = (10.6 \pm 16.0)$ AU km s^{-1}, one may conclude that low-speed solar wind is forced to corotate with the sun out to larger heliocentric distances. The Alfvénic radius inferred from these data is $r_A \approx 30\ R_S$. A more detailed discussion of inferences about the Alfvén critical point from solar wind angular momentum as observed by Helios can be found in the paper by *Marsch and Richter* [1984].

Figure 2 displays in the top panel the angular momentum loss rate of the sun, $\dot{M}L$ (or the angular momentum carried away by the solar wind), and the magnetic field flux F_B (bottom) versus heliocentric distance. The quantity $\dot{M}L$ exhibits the same trend as L itself. For a more detailed discussion we again refer to *Pizzo et al.* [1983]. The bottom part of Figure 2 shows that within the large error bars there appears no significant trend in F_B as a function of flow speed. There is a weak indication for F_B to be somewhat higher in the intermediate-speed regime corresponding to stream interaction zones and trailing edges of fast streams. However, it seems reasonable to state that within measurement uncertainty, r^2B_r is fairly well conserved with a total average of $F_B = (3.28 \pm 1.67)$ nT AU^2 sr^{-1}. A comment on our error analysis is in order here: We quoted standard deviations instead of the error of the mean itself in the figures and tables. The errors of the means are certainly much smaller (by about a factor of 94 for the entire data of our 8873 spectra) than their standard deviations for all the data bins. However, in

TABLE 1. Conserved Quantities Averaged Over Heliocentric Distance

	$v_p < 400$ km s^{-1}	400 km s$^{-1} \le v_p \le$ 600 km s^{-1}	600 km s$^{-1} < v_p$	Total
$\dot{M}$, 10^{11} g s^{-1} sr^{-1}	1.49 ± 0.61	1.09 ± 0.62	0.81 ± 0.22	1.02 ± 0.53
L, AU km s^{-1}	10.6 ± 16.0	2.34 ± 17.0	−1.55 ± 20.85	1.71 ± 19.11
$\dot{M}L$, 10^{30} dyn cm sr^{-1}	2.59 ± 4.66	0.56 ± 4.36	−0.37 ± 2.91	0.42 ± 3.95
ε, (100 km s^{-1})^2	6.86 ± 1.08	13.65 ± 3.49	24.18 ± 3.49	17.4 ± 7.2
$\dot{M}\varepsilon$, 10^{26} ergs s^{-1} sr^{-1}	1.03 ± 0.47	1.42 ± 0.68	1.94 ± 0.56	1.60 ± 0.68
F_B, nT AU^2 sr^{-1}	2.86 ± 1.87	3.54 ± 1.73	3.15 ± 1.49	3.28 ± 1.67
$\dot{M}(\varepsilon + \frac{1}{2}v_\infty{}^2)$, 10^{26} ergs s^{-1} sr^{-1}	3.88 ± 1.61	3.51 ± 1.79	3.48 ± 0.94	3.55 ± 1.45
u_ϕ, km s^{-1}	11.82 ± 18.12	1.80 ± 21.16	−2.02 ± 34.83	1.45 ± 28.11

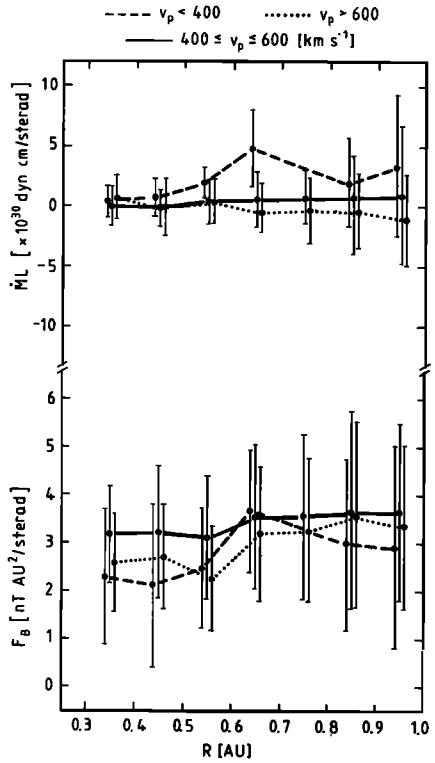

Fig. 2. Total angular momentum flux ($\dot{M}L$) and magnetic flux (F_B) versus heliocentric distance for various ranges of solar wind flow speed.

view of the temporal and spatial variability of the solar wind we thought that the respective errors of the mean are somewhat overoptimistic and less informative than their standard deviations.

Figure 3 presents a survey of the energy per amu (ε) carried by a solar wind plasma parcel, the mass flux ($\dot{M}$), and energy flux ($\dot{M}\varepsilon$) of the wind, or equivalently, the total mass and energy loss rate of the sun per steradian in the ecliptic plane. The three quantities are plotted on logarithmic scales versus heliocentric solar distance. Points have been connected by straight lines to guide the eye. Note that all quantities are surprisingly constant. Standard deviation bars are largest for the intermediate-speed regime. There is some overlapping between the various groups of lines within the error bars, but a systematic dependence on flow speed is obvious: ε increases with increasing bulk velocity. This is due to the fact that even at 0.3 AU the total internal energy never contributes more than 10% to ε. Therefore ε is almost identical to $0.5u_r^2$. The mass flux in the intermediate panel shows the reversed trend, with highest fluxes in the slow-speed wind often corresponding (for the time period under consideration) to plasma nearby the heliospheric current sheet and magnetic sector boundaries. These general trends are known from 1-AU observations [*Feldman et al.*, 1977].

By multiplying $\dot{M}$ and ε one obtains the total energy flux of the solar wind. Notice, however, that the gravitational potential is only defined within an integration constant that can be chosen as the potential difference $\Delta\phi$ between infinity and the solar surface. $\Delta\phi = \phi_G(\infty) - \phi_G(R_S) = 0.5v_\infty^2$ according to (A17). This constant does not alter the top part of Figure 3, as only a shift in the scale for ε results. However, $\Delta\phi$ has an impact on the total energy flux, as the mass flux varies with the solar wind speed and thus also the flux of potential energy. Therefore the last panel explicitly displays the quantity $\dot{M}(\varepsilon + \frac{1}{2}v_\infty^2)$. This quantity is remarkably constant and within the error bars even independent of the flow speed. This result has not been obtained in this explicit form before from, for example, the IMP data [*Feldman et al.*, 1977]. In case of the Helios observations, *Schwenn* [1983] has shown that the total energy flux seems to be a universal constant and remarkably insensitive to the bulk speed. He did not include the alpha particles in his analysis. However, his statistical basis comprised more than 2.5×10^6 spectra. Thus it is now experimentally fairly well established, at least between 0.3 and 1 AU, that the energy supplied by the sun per second to create the highly structured solar wind is a global constant and not associated with the stream structure itself.

We should also sound a note of caution concerning the above claimed conservation of the total energy flux. Standard

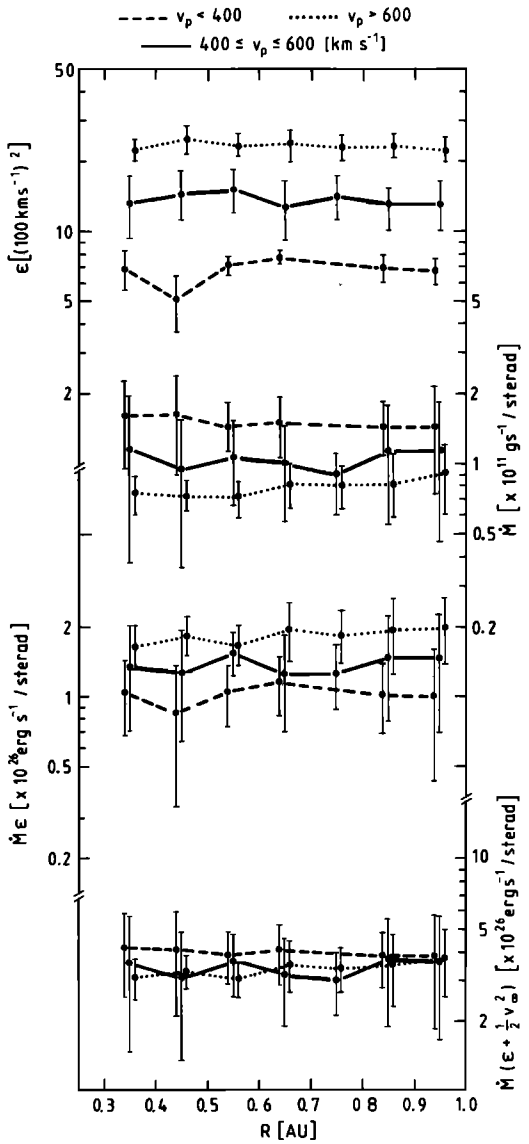

Fig. 3. Quantities conserved for solar wind flow in the ecliptic plane with local spherical symmetry: energy per amu or total energy flux divided by the mass flux (ε), mass loss rate of the sun or total mass flux ($\dot{M}$), flux of kinetic and potential energy ($\dot{M}\varepsilon$), and total energy flux, including the flux of gravitational potential energy with respect of the solar surface. All parameters are displayed (on various scales) versus radial distance for three solar wind speed classes.

TABLE 2. Dimensionless Numbers Characterizing the Total Internal Energy State

	$v_p < 400$ km s^{-1}	400 km s^{-1} $< v_p <$ 600 km s^{-1}	600 km s^{-1} $< v_p$	Total
A	0.92 ± 0.03	0.88 ± 0.07	0.91 ± 0.03	0.90 ± 0.02
$\beta_\parallel$	3.41 ± 4.11	2.05 ± 2.88	1.32 ± 0.81	1.91 ± 2.55
$\beta_\perp$	3.12 ± 4.42	1.69 ± 2.83	1.11 ± 1.04	1.63 ± 2.63
$\alpha_\parallel$	0.57 ± 0.53	0.55 ± 0.42	0.28 ± 0.20	0.44 ± 0.38
$\alpha_\perp$ (20%)	0.086 ± 0.085	0.095 ± 0.078	0.042 ± 0.036	0.071 ± 0.069
γ	1.59 ± 0.09	1.62 ± 0.09	1.67 ± 0.08	1.64 ± 0.09

deviation bars are large, and within the Helios orbital range, ε is entirely dominated by the contribution of the bulk kinetic energy per amu, i.e., by the term $0.5u_r^2$. For a typical high-speed lineup of the Helios probes, *Schwartz and Marsch* [1983] have given a detailed presentation of the various contributions to ε in terms of species and internal degrees of freedom. For 1 AU the corresponding numbers are contained in the article by *Feldman et al.* [1977, Table 5]. The division of ε into its four important constituents according to (2) is discussed in section 2.4. Also the potentials ϕ_T and ϕ_Ω are then defined and investigated in detail. The contribution of the internal energy to ε seldom reaches more than 5% at 1 AU; however, at 0.3 AU its contribution to ε can amount to up to 10%.

2.3. *The Radial Evolution of Internal Energy*

In this section we discuss Helios observations characterizing the internal energy state of the electron-proton–alpha particle plasma of the solar wind. Typical figures for the characteristic parameters shown below are summarized in Tables 2 and 3. Figure 4 shows the radial dependence of the effective thermal speeds that are based on the total pressures parallel and perpendicular to the magnetic field direction, i.e., $v_{\|,\perp}=(p_{\|,\perp}/\rho)^{1/2}$ (as defined in (A10*a*) and (A10*b*); note that particularly in high-velocity streams, the alpha-proton differential speeds $u_{\alpha,p}$ contribute to the total parallel pressure). The last panel displays the speed $v_Q = (Q_r/\rho u_r)^{1/2}$. The term v_Q^2 represents the heat flux contribution to ε (compare with (A15)). Note that in a heat flux driven solar wind model one would expect v_Q^2 to be the leading term in ε at 1 R_S and to be of the order of $\frac{1}{2}u_\infty^2$ if the major part of the asymptotic kinetic energy originates from the coronal heat flux. As can be seen from Figure 4, v_Q is by about a factor of 2 smaller than $v_{\|,\perp}$ for all heliocentric distances accessible to the Helios probes. In approaching the sun a general trend for all velocities to increase is clearly visible. This tendency is certainly statistically significant for $v_{\|,\perp}$, since the standard deviations are small. A similar trend in v_Q is less distinct, as the lines are closer to each other and as there is considerable overlapping within the standard deviation bars. Note also that v_Q shows the reverse trend as compared with $v_{\|,\perp}$ in its dependence on the bulk speed. Whereas in high-speed solar wind the effective thermal speeds are largest, the opposite is true for v_Q. In a subsequent figure we show that the reason for this feature is that the total heat flux is largest in slow solar wind, at least in perihelion at 0.3 AU.

We would like to emphasize again that $v_{\|,\perp}$ are based on the total pressures $p_{\|,\perp}$ and thus also contain the contribution from the electron pressure. Summing over all the particle species smooths out the individual anisotropies and also weakens the gradients somewhat. For example, proton and alpha temperatures parallel and perpendicular to the magnetic field exhibit different radial trends [*Marsch et al.*, 1982*a*, *b*]. Furthermore, the electron distributions in general yield $T_{e\|} > T_{e\perp}$ [*Feldman et al.*, 1975, 1977; *Pilipp*, 1983], whereas high-speed protons often show $T_{p\|} < T_{p\perp}$ [*Feldman et al.*, 1973; *Marsch et al.*, 1982*a*]. Averaging over these opposite anisotropies results in a net total pressure anisotropy that is less pronounced than the anisotropies in the individual particle distributions.

This finding is displayed in the top part of Figure 5, which

TABLE 3. Parameters Characterizing the Internal Energy at 0.35 AU (0.95 AU)

	$v_p < 400$ km s^{-1}	400 km s^{-1} $< v_p <$ 600 km s^{-1}	600 km s^{-1} $< v_p$
$v_\parallel$, km s^{-1}	55.0 ± 10.9	67.4 ± 14.4	81.5 ± 8.8
	(38.6 ± 5.5)	(53.4 ± 8.3)	(60.4 ± 5.6)
$v_\perp$, km s^{-1}	50.1 ± 5.3	60.2 ± 10.6	76.0 ± 7.2
	(35.9 ± 4.9)	(46.9 ± 7.2)	(53.2 ± 4.6)
v_Q, km s^{-1}	33.7 ± 23.9	38.4 ± 18.2	29.3 ± 10.2
	(18.5 ± 13.1)	(29.2 ± 12.9)	(24.8 ± 10.8)
Q, 10^{-2} erg cm^{-2} s^{-1}	9.38 ± 8.14	5.99 ± 4.14	3.37 ± 1.44
	(0.51 ± 0.48)	(0.73 ± 0.44)	(0.51 ± 0.31)
Q_t, 10^{-3} erg cm^{-2} s^{-1}	2.52 ± 3.31	5.70 ± 6.21	10.62 ± 5.79
	(0.09 ± 0.11)	(0.24 ± 0.31)	(0.33 ± 0.20)
u_α, km s^{-1}	11.6 ± 27.8	51.9 ± 48.2	98.5 ± 44.5
	(−1.4 ± 7.1)	(15.9 ± 19.9)	(31.5 ± 26.4)
u_p, km s^{-1}	−1.16 ± 4.38	−5.01 ± 5.09	−9.45 ± 4.76
	(0.12 ± 0.57)	(−2.09 ± 2.69)	(−4.48 ± 4.01)
ϕ_T, (100 km s^{-1})^2	0.99 ± 0.42	1.32 ± 0.45	1.67 ± 0.31
	(0.39 ± 0.15)	(0.74 ± 0.20)	(0.86 ± 0.15)
ϕ_Ω, (100 km s^{-1})^2	0.15 ± 0.29	0.20 ± 0.26	0.54 ± 0.56
	(0.11 ± 0.10)	(0.13 ± 0.15)	(0.18 ± 0.17)
v_A, km s^{-1}	74.8 ± 43.4	111.9 ± 47.8	131.5 ± 29.3
	(41.5 ± 14.8)	(55.9 ± 17.6)	(68.3 ± 12.5)

Values in parentheses are for 0.95 AU.

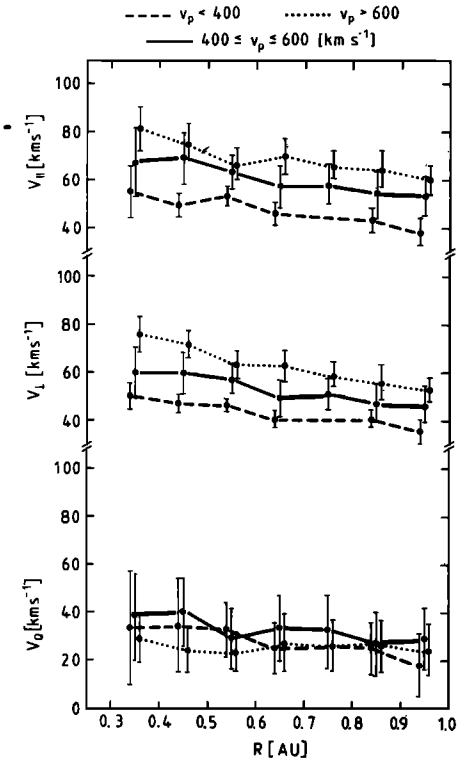

Fig. 4. Effective thermal speeds $v_{\parallel,\perp} = (p_{\parallel,\perp}/\rho)^{1/2}$ and the speed $v_Q = (Q_r/\rho u_r)^{1/2}$ plotted versus heliocentric distance for high (dotted curve), intermediate (solid curve), and low (dashed curve) solar wind speeds. Error bars refer to the standard deviations of the mean for each radial distance bin of 0.1 AU in width.

shows the ratio $A = (v_\perp/v_\parallel)^2$ (the thermal pressure ratio) versus radial heliocentric distance. The bottom part displays $\beta_\parallel$, the ratio between parallel thermal pressure and magnetic pressure. The ratio A typically amounts to 0.9 and, surprisingly, seems to be somewhat higher in fast than in slow streams, although this trend is not very significant. The declining course for the curve corresponding to fast wind is compatible with the radial trend in the proton anisotropy. Since in high-speed streams the proton temperature is higher than the electron temperature [*Feldman et al.*, 1976], the protons dominate the total pressure there and thus mostly determine its anisotropy.

The ratio $\beta_\parallel$ exhibits much larger standard deviations than the ratio A, since the rather large measurement uncertainty of the ion densities enters linearly into $\beta_\parallel$, whereas it cancels out in A. The data suggest a slightly increasing trend in $\beta_\parallel$ with solar radial distance, although this might appear spurious considering the large standard deviation bars. The plot for $\beta_\perp$ resembles very much that for $\beta_\parallel$ and thus is not shown here. Averaged values for $\beta_\parallel$ and $\beta_\perp$ can be found in Table 2. We find $\beta_\parallel = 1.91 \pm 2.55$ and $\beta_\perp = 1.63 \pm 2.63$, in good agreement with earlier estimates [*Feldman et al.*, 1977].

In discussing Figure 4 we mentioned already that the total heat flux is largest in slow-speed solar wind. This result is detailed in Figure 6, which shows the total heat flux Q (top) and the ion heat flux Q_i (bottom) versus solar radial distance. Note that all heat fluxes are plotted logarithmically and that Q_i amounts to less than 10% of the total Q. Thus Q is basically identical with the electron heat flux Q_e. Q and Q_i decrease by about or even more than an order of magnitude between 0.3 and 1 AU. Most of this decline is due to the steeply decreasing mass flux, since, as demonstrated in Figure 4, $v_Q^2 = Q_r/\rho u_r$ is almost constant. We do not want to go into the details of the microstructure of the electron distribution giving rise to a field-aligned skewness [*Feldman et al.*, 1975; *Rosenbauer et al.*, 1977] but only want to point out that Q_e is somewhat smaller in fast solar wind streams, at least in perihelion, than in slow wind despite the fact that the so-called electron strahl [*Rosenbauer et al.*, 1976] is most pronounced in fast streams [*Pilipp et al.*, 1981]. Note, however, the extensive discussion by *Pilipp* [1983] indicating that microscopic features in electron distribution more distinctly correlate with the magnetic sector structure than with the ion stream structure.

Let us concentrate now on the bottom part of Figure 6. As mentioned before, Q_i represents only a minor part of Q, which is dominated by the electrons. However, there are some interesting details that are worth mentioning. Close inspection of the curves shows that Q_i exhibits a trend opposite to Q_e. Largest values are observed in fast streams, and lowest total ion heat fluxes occur in slow wind. There is twofold reason for this. First, the intrinsic proton and alpha particle heat fluxes [cf. *Marsch et al.*, 1983, Figure 4] show exactly the same trend. They also steeply increase toward the sun. Second, as can be seen from the definition in (A12), and (A13), also enthalphy fluxes related to the species motion relative to the center of mass enter in Q_i. Ion differential speeds are most developed in high-velocity streams [*Asbridge et al.*, 1976] and closely trace the local Alfvén speed [*Marsch et al.*, 1982*b*]. These two features of the internal structure of ion distributions cause the radial trend as summarized in Figure 6 and also explain why Q_i increases with the solar wind velocity.

The ion speeds relative to the center of mass frame are depicted in Figure 7, which shows u_α and u_p in kilometers per

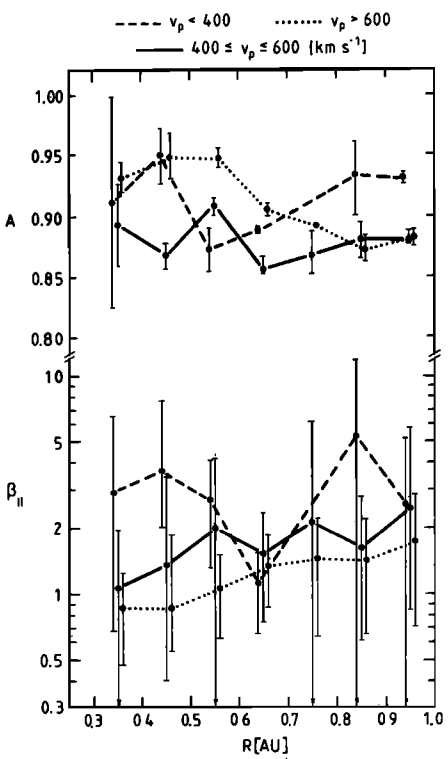

Fig. 5. Ratio (A) of total thermal pressures perpendicular and parallel to the magnetic field and ratio ($\beta_\parallel$) of the parallel thermal pressure to the magnetic field pressure shown as a function of radial distance in AU.

second versus heliocentric distance. The aforementioned trend is obvious. Note that the speed difference can be large at 0.3 AU with $\Delta v_{\alpha p} = u_\alpha - u_p \approx 110$ km s^{-1} compared with a corresponding Alfvén speed of $v_A = 130$ km s^{-1}. A detailed review on the ion differential speed phenomenon is given by *Neugebauer* [1981]. Although the shift of the protons back to the sun in the solar wind frame is only a few kilometers, per second, it has to be taken into account in balancing the oppositely directed proton heat flux. This aspect has been elucidated by *Schwartz and Marsch* [1983] in their lineup study on the radial evolution of internal ion energy. If the trend continues that $\Delta v_{\alpha p}$ traces roughly the Alfvén speed, the contribution of Q_i to the total heat flux might become quite large, as the Alfvén speed further increases in approaching the sun. Similarly, the anisotropy stresses in the total pressure might increase closer to the solar corona. However, since the true course of $\Delta v_{\alpha p}$ has not been observed directly below 0.3 AU and since too little is known about this important region, we shall not pursue our speculation further. However, we would like to stress the possible important role played by the proton-alpha differential speed for the evolution of the internal ion energy.

The final topic in this section is the discussion of the effective polytropic index γ, as defined in (A21), in order to cast the thermal potential ϕ_T in a form (equation (A22)) that resembles the expression for a polytropic equation of state. Besides the pressure ratio A, also the quantities $\alpha_{\|,\perp}$, defined in (A19) and referred to as normalized heat fluxes, enter the formula for γ in the combination $\frac{1}{2}(\alpha_\| + 2A\alpha_\perp) = (v_Q/v_\|)^2$. Thus $\alpha_{\|,\perp}$ resembles in character the quantities A and $\beta_{\|,\perp}$, all of which are defined as squared ratios of typical MHD speeds in the plasma. By definition, $\alpha_{\|,\perp}$ are based on known quantities that can be estimated from in situ measurements. Unfortunately, the two intrinsic heat flux components $q_\|$ and $q_\perp$ have not been calculated separately on a routine basis in the Helios data analysis. Inspection of individual spectra of electrons (W. G. Pilipp, private communication, 1983) and ions yield ratios of $q_\perp/q_\|$ between a few percent and about 30%. The top part of Figure 8 shows $\alpha_\|$ in our standard format versus radial distance from the sun. Here we used $\alpha_\perp = 0.2\ \alpha_\|$. The course for $\alpha_\perp$ is very similar to $\alpha_\|$ (since the total heat flux is dominated by the intrinsic electron heat flux) and thus not shown explicitly. Note the logarithmic scale for $\alpha_\|$ and the fairly large standard deviation bars. Numerical parameters are given in Table 2.

According to Figure 8, $\alpha_\|$ varies typically between 0.1 and 1 and attains its smallest values in high-speed wind. This reflects the dependence of the total heat flux on bulk speed, as demonstrated in Figure 6. Also, the larger thermal speed in high-velocity solar wind streams results in relatively small values of $\alpha_\|$. However, in view of the pronounced radial variations of the mass flux ($\sim r^{-2}$, see Figure 3) and of the total heat flux one finds $\alpha_\|$ to be remarkably insensitive to heliocentric distance. The same holds for v_Q, plotted in Figure 4; v_Q exhibits an even weaker dependence on the bulk speed than $\alpha_\|$.

It should be noted in this context that an α_e parameter similar to ours has been introduced phenomenologically by *Hollweg* [1976] in order to establish an electron heat flux law

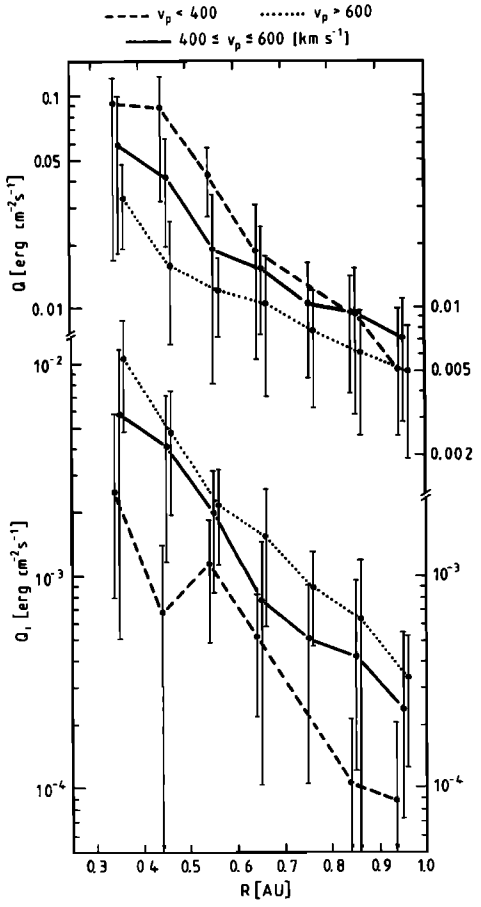

Fig. 6. Total heat flux (Q) of the multicomponent plasma with respect to the center of mass frame (top) and the corresponding total ion heat flux (bottom) are shown in dependence upon heliocentric distance for three solar wind speed classes. Note the different logarithmic scales for the heat fluxes.

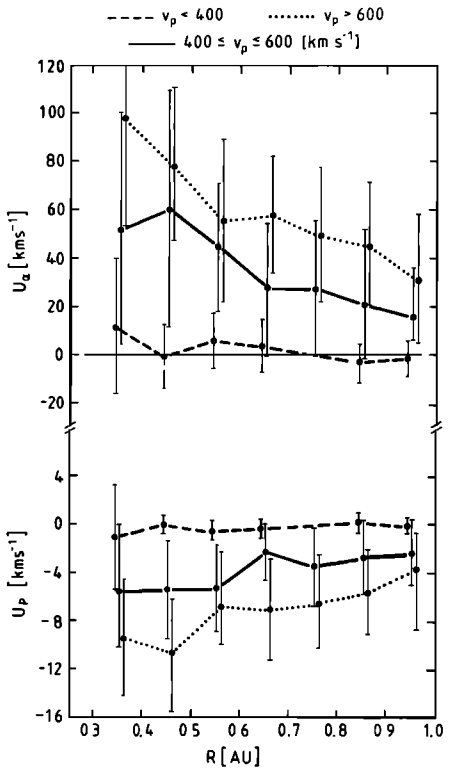

Fig. 7. Ionic speeds relative to the center of mass frame (solar wind bulk frame) for alphas (top) and protons (bottom) versus heliocentric distance for various solar wind velocities.

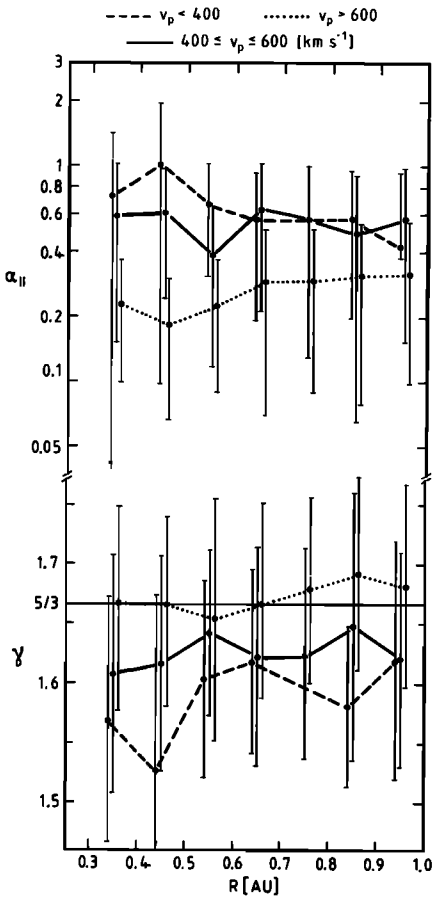

Fig. 8. Parallel component of the normalized total heat flux ($\alpha_{\parallel}$, top) and effective polytropic index (γ, bottom) versus heliocentric distance. Note that γ is almost equal to $\frac{5}{3}$ in high-speed solar wind.

in the collisionless regime of the solar wind expansion where the classical heat conduction law [*Spitzer*, 1962] due to Coulomb collision does not apply any more. In accordance with Figure 8, *Hollweg* [1976] estimated his α_e to be of order unity or slightly below. Certainly, the numerical values of $\alpha_{\parallel,\perp}$, as defined in the appendix, depend on the detailed shape of the electron and ion distribution functions that theoretically can correctly be described only within the framework of kinetic theory. All that is required in our fluid model, however, is the heat flux itself, which may originate from a variety of underlying features in the electron distribution, such as an exospheric "strahl" [*Rosenbauer et al.*, 1976] or simply a slight skewness in the thermal regime. Since our estimate of $\alpha_{\parallel,\perp}$ is based on the overall measured distribution, it automatically includes all these features. As an empirical parameter $\alpha_{\parallel,\perp}$ is fairly general and may be used irrespective of the detailed microphysics of the heat conduction.

The pressure ratio A and the quantities $\alpha_{\parallel,\perp}$ or v_Q are the basic parameters of the polytropic index γ that may also be expressed by (see equations (A19)–(A21))

$$1/(\gamma - 1) = (1 + 2A)/2 + (v_Q/v_{\parallel})^2 \qquad (1)$$

This emphasizes the importance of v_Q, displayed in Figure 4. An inspection of Figure 8 shows that γ is fairly insensitive to the distance from the sun. Within the standard deviation bars no significant radial trend appears. Obviously, the γ values corresponding to fast solar wind closely approach the canonical value of $\frac{5}{3}$, associated with isotropic, adiabatic expansion. This is very surprising in view of the variety of nonthermal characteristics in the ion [*Marsch et al.*, 1982*a*, *b*] and electron [*Feldman et al.*, 1975; *Pilipp*, 1983] distribution functions in high-speed streams. On the other hand γ, as define in (1), depends only on the characteristics of the overall particle distribution function composited by all the different particle species considered here. Figure 8 clearly demonstrates that from a dynamical point of view the heat flux is of rather minor importance between 0.3 and 1 AU. If the degradation of the generalized heat flux of the solar wind electrons and ions could actually be considered to be the only interplanetary source of internal particle energy, we might conclude that the high-velocity plasma expands almost adiabatically beyond 0.3 AU. But there exist other possible sources of nonadiabaticity. Wave turbulence is the most obvious example. We do not intend to address this complicated topic here and must therefore admit that our present data do not allow a final statement about adiabaticity. Our findings indicate, however, that even the comparatively close approach of the Helios probes to the sun is still far too distant in order to detect directly any influence of the electron heat flux, as the most prominent term in Q, on the bulk dynamics of the fast solar wind.

From Figure 8 we find that in low-speed wind, on average, $\gamma \approx 1.6 \pm 0.1$, which is somewhat smaller than the adiabatic value. This is due to the fact that the heat flux and thus v_Q are generally larger in slow than in fast streams (see again Figures 4 and 6). Numerical parameters are given in Table 3. Taking the γ value averaged over our total data set as $\gamma = 1.64 \pm 0.1$, one might claim that at least within the Helios orbital range an isotropic, adiabatic equation of state for the total plasma pressure could possibly exist. This result is remarkable insofar as the diverging field geometry generally tends to produce anisotropies in the pressure that can only be counterbalanced by Coulomb collisions or other anomalous collisional isotropization effects. Indeed, Coulomb collisions are able to isotropize major parts of the electron distribution, as inferred in a paper by *Ogilvie and Scudder* [1978]. However, they are unable to prevent the formation of heat flux carrying high-energy (exospheric) tails, as shown in a paper by *Lemons and Feldman* [1983]. The same comment applies to the ions. *Marsch and Goldstein* [1983] have shown that central parts of proton distributions are at times effectively isotropized by Coulomb collisions, although the formation of double peaks and heat flux shoulders cannot be prevented by collisions. In addition to Coulomb collisions, a variety of plasma microinstabilities [*Schwarz*, 1980] can limit the formation of pronounced anisotropies and third-order moments. Nevertheless, a complete understanding of the combined action of all these dissipative processes on the composite particle distribution has not yet been achieved.

2.4. *Kinetic Energy and Potentials*

In order to enable a separate discussion of the different physical terms leading as a sum to a coronal expansion (within a multicomponent, anisotropic, yet one-fluid, thermally driven solar wind model), we may introduce the following scenario. The radially expanding corona is visualized in terms of the motion of a single particle (its kinetic energy per amu is $\frac{1}{2}u_r^2$) retained by the binding solar gravitational potential and accelerated away from the sun by forces arising from the magnetorotational potential ϕ_Ω (comprising azimuthal kinetic energy and Poynting flux) and the thermal potential ϕ_T (comprising enthalpy and heat flux). Actually, these potentials involve the self-consistent density compatible with a given

mass loss rate $\dot{M}$. They should thus be written as $\phi_\Omega(\rho(r), r)$ and $\phi_T(\rho(r), r)$ to indicate the dependence on the local plasma density. The total energy per amu, ε, is a conserved quantity

$$\varepsilon = \tfrac{1}{2} u_r^2 + \phi_\Omega + \phi_T + \phi_G \qquad (2)$$

Since the gravitational potential represents an external force acting on the wind, ϕ_G does only depend on heliocentric distance. It is given in the appendix by (A17). The other potentials are detailed in measurable quantities in (A16) and (A18) of the appendix. They depend in a self-consistent fashion on the bulk flow parameters and intrinsic thermal properties of the wind. In the subsequent figures we plotted the four terms adding up to ε versus radial solar distance. We have already displayed ε itself in Figure 3. It is again recalled to the reader that in terms of fluid quantities, ε is the total energy flux divided by the mass flux. This quantity is most relevant for determining the radial flow speed u_r, for example, at 1 AU [*Holzer and Leer*, 1980].

In Figures 9*a*–9*c* we show the bulk kinetic energy of the radial flow as well as the thermal, magnetorotational, and gravitational potential against solar radial distance and for the three different solar wind speed classes separately. Note that scales for $\frac{1}{2}u_r^2$ are different, since this term dominates the others by more than an order of magnitude. For all speed regimes the potential ϕ_Ω almost compensates the negative gravitational potential ϕ_G, which is weak only at distances larger than 0.3 AU, where the escape velocity to infinity is about 77 km s^{-1} compared with 618 km s^{-1} at the solar surface. If we write ϕ_Ω in equivalent speeds as $\phi_\Omega = \frac{1}{2}v_\Omega^2$, we would find from Figure 9 that $v_\Omega \approx 30$–60 km s^{-1}. The potential ϕ_Ω is almost constant between 0.3 and 1 AU. The reason is that for $r \gg r_A$ according to (A16) ϕ_Ω is dominated by $B_\phi^2/4\pi\rho$, i.e., the azimuthal Alfvén velocity squared, which is roughly constant. There is slight trend for ϕ_Ω to increase with bulk speed at a fixed radial distance, particularly in Figure 9*c*.

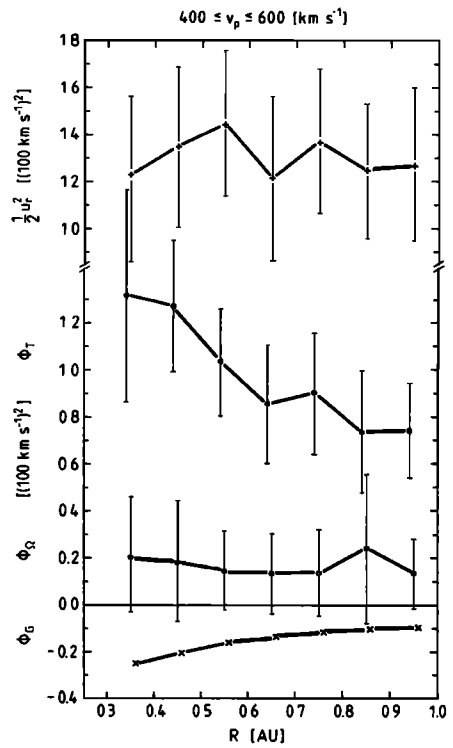

Fig. 9*b*. Constituents of ε versus radial distance from the sun for intermediate flow speeds of the protons ($400 \le v_p \le 600$ km s^{-1}). The format is the same as that used in Figure 9*a*.

However, this trend is based on poor statistical ground because of the large standard deviation bars. These arise from the large mesaurement uncertainties in u_ϕ and B_ϕ that enter ϕ_Ω. They possibly also reflect wave turbulence that tends to produce larger average values of u_ϕ and B_ϕ than can be ex-

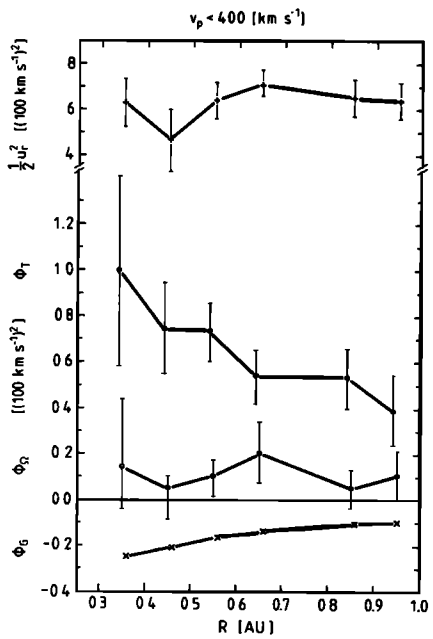

Fig. 9*a*. Kinetic energy per amu associated with the radial bulk velocity component and the three potentials that constitute the conserved quantity ε. All parameters are given in (100 km s^{-1})^2 and are plotted versus heliocentric distance in AU. This figure corresponds to proton flow speeds below 400 km s^{-1}.

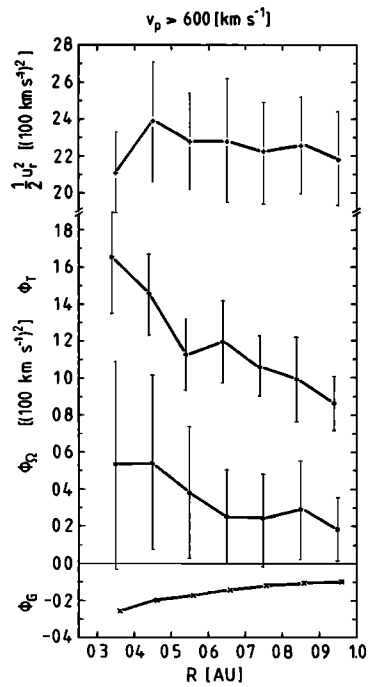

Fig. 9*c*. Kinetic energy per amu and potentials for high-speed flows ($v_p > 600$ km s^{-1}) in a format similar to that used in Figure 9*a* but with slightly different scales.

pected from the smooth numbers pertaining to the Parker spiral within the WD model. Nevertheless, taking the measurements at face value, on could infer an increasing trend for ϕ_Ω in high-speed streams (Figure 9c), as when approaching the sun. By theoretical arguments we expect, however, ϕ_Ω never to become comparable with, say, ϕ_T. Thus the radial acceleration of the solar wind by the magnetorotational potential is negligible as compared with thermal pressure gradient forces. Namely, in a theoretical paper, *Barnes* [1974] investigated the Poynting flux associated with the spiral magnetic field (which is one ingredient of ϕ_Ω) and theoretically concluded that the magnetic forces cannot achieve significant radial acceleration.

If the real solar wind is required to start with a velocity $u_r = 0$ somewhere deep in the corona, there remains only the thermal potential as to both lift the plasma out of the restraining gravitational trough and accelerate it up to the in situ observed velocity u_r. The bulk kinetic energy of radial motion and the thermal potential ϕ_T are plotted in Figures 9a–9c for the various speed regimes. The term $\frac{1}{2}u_r^2$ is found to be fairly constant without any distinct trend. Typical values for the kinetic energy are given in Table 1. Note that scales are different for ϕ_T and $\frac{1}{2}u_r^2$. The respective second panel in Figure 9 shows the thermal potential, which is almost equal to $\phi_T = \gamma/(\gamma - 1)v_{||}^2$ according to (A22) and the results in Figure 5 ($A \approx 0.9$). Since we found γ to be close to $\frac{5}{3}$ for all speed classes (see Figure 8), we may conclude that ϕ_T is almost equal to $\frac{5}{2}V_{||}^2$ within the orbital range of Helios. The thermal potential ϕ_T progressively increases with decreasing heliocentric distance by a factor of about 2 between 1.0 and 0.3 AU. This trend is statistically significant for the three solar wind speed classes. In the perihelion a ϕ_T of about 10% of $\frac{1}{2}u_r^2$ is typical.

3. SUMMARY AND CONCLUSIONS

We have investigated bulk and internal energy plasma parameters of the solar wind based on the Helios data set covering heliocentric distances between 0.3 and 1 AU. Our study was guided by theoretical ideas developed in many theoretical papers, quoted in the introduction, in which models for a thermally driven, multicomponent, and anisotropic solar wind have been developed. We need to keep in mind the many limitations and possible sources of inaccuracy in our data set. Mean values for the relevant parameters and corresponding standard deviations are given in Tables 1, 2, and 3. Our main observational findings are listed below.

1. Total angular momentum flux $\dot{M}L$ is the range of $(0.42 \pm 3.95) \times 10^{30}$ dyn cm sr^{-1} for our limited data set. This figure is in accordance with a more comprehensive study by *Pizzo et al.* [1983].

2. In accordance with Gauss' law we find $F_B = r^2 B_r$ to be rather constant and not very sensitive to heliocentric distance and flow speed with a total average of $F_B = (3.28 \pm 1.67)$ nT (AU)^2 sr^{-1}.

3. Within experimental uncertainties the expected invariants ε, $\dot{M}$, $\dot{M}\varepsilon$, and $\dot{M}(\varepsilon - \phi_G(R_S))$ are actually found to be fairly constant. The total energy per amu, ε, is extremely well conserved in high-velocity streams. With the exception of the last quantity the other invariants are dependent on solar wind flow velocity and confirm the typical trends reported from 1-AU observations [*Feldman et al.*, 1977].

4. If one converts the mass loss rate of the sun (average $\dot{M} = (1.02 \pm 0.53) \times 10^{11}$ g s^{-1} sr^{-1}) into an ion number density flux at 1 AU, one finds for $j_E = n_E u_{rE}$ a very narrow range of $2 \lessapprox j_E \lessapprox 4 \times 10^8$ cm^{-2} s^{-1}. This is one of the best established observational constraints on solar wind expansion (see also *Leer and Holzer* [1979]).

5. The total energy flux $\dot{M}(\varepsilon + \frac{1}{2}v_\infty^2) = S_T$ is surprisingly constant and independent of flow velocity. This result has also been established with much larger statistical significance by *Schwenn* [1983]. For our limited data set we find $S_T = (3.55 \pm 1.45) \times 10^{26}$ ergs s^{-1} sr^{-1}. This uniformity of S_T may have an important, yet unknown physical reason.

6. The total pressure anisotropy of the multicomponent (electron, proton, alpha particle) plasma turns out to be close to 1. We find $A = 0.9$ and only a weak dependence on flow speed. This does not necessarily imply isotropic partial pressures of the individual constituents. But it suggests that within the one-fluid picture of the solar wind an isotropic total pressure is a reasonable assumption in modeling the flow, at least between 0.3 and 1 AU.

7. Particle heat fluxes exhibit strong radial gradients and vary considerably with the solar wind speed. The contribution of the ions (double peaks and ion differential streaming) to the total heat flux never exceeds 10% within the Helios orbital range. The expression $v_Q^2 = Q_r/\rho u_r$ is the quantity to be compared with the specific kinetic energy $\frac{1}{2}u_r^2$. The speed v_Q turns out to be only weakly dependent on flow speed and varies smoothly with radius with a typical total average of $v_Q = (28.4 \pm 13.3)$ km s^{-1}. This value is less than any thermal speed, and it indicates that the heat flux is without dynamical importance for the wind expansion within 0.3 and 1 AU. This result may also be expressed in terms of a polytropic index γ.

8. The polytropic index γ, as defined in (1), is within its errors equal to $\frac{5}{3}$ and somewhat smaller in slow wind. Thus from the Helios observations we find the rather interesting result that the high-speed plasma seems to expand nearly adiabatically between 0.3 and 1 AU with an almost isotropic total pressure, as far as only the degradation of the heat flux is accounted for as a possible interplanetary source of internal energy. However, there may be other sources (wave turbulence) that could lead to a nonadiabatic behavior.

9. A brief discussion of the solar wind expansion has been given, whereby the analogy with a single particle moving in various potentials provides a transparent picture to understand the dynamics. The most significant radial trend is observed in the thermal potential ϕ_T, which increases by about a factor of 2 in approaching the sun. As expected from theoretical arguments, the magnetorotational potential ϕ_Ω is comparatively small and only about sufficient as to compensate the negative gravitational potential, which is rather weak within the Helios orbital range from 0.3 to 1 AU.

Finally, we address a point in which the reader could possibly see a contradiction between the results of Figure 4 and 8. The polytropic index γ has been evaluated spectrum by spectrum as a local parameter and has then been averaged over heliocentric distance. Since we find $\gamma \approx \frac{5}{3}$, we would conclude that adiabaticity prevails if no sources of internal energy other than heat flux degradation existed in the interplanetary medium. If we assume for the moment this to be the case, then we expect the thermal speeds to vary as $v_{||}^2 = v_\perp^2 \sim \rho^{\gamma-1} = \rho^{2/3}$ with local density, and consequently $v_{||} \sim R^{-2/3}$ for a density dependence such as R^{-2} on heliocentric distance. This, however is not what Figure 4 shows. A least squares fit yields a power law dependence $v_{||,\perp} \sim R^\delta$ with δ ranging between $-(0.3$–$0.4)$, which is smaller than the adiabatic value of -0.66 by almost a factor of 2. However, the conclusion that these

observations indicate that the plasma behaves nonadiabatically is not as obvious as it might appear at a first glance. The real solar wind as actually measured by Helios is highly structured, and the data sampled in the radial distance bins of Figure 4 are associated with different flux tubes. This fact can seriously bias the results if a polytropic index is indirectly inferred from the radial plot of $v_{\|,\perp}$ in Figure 4.

We may estimate the power law index δ for the radial temperature plot from the formula

$$\delta = \ln (v_{\|1}/v_{\|2})/\ln (R_1/R_2) \tag{3}$$

where $R_1 > R_2$ without loss of generality and $v_{\|1,2}$ are the thermal speeds as measured at the heliocentric distance $R_{1,2}$. Let us assume that a polytropic equation of state with index γ exists, and thus locally we have

$$v_\|^2 = v_{\|0}^2(\rho/\rho_0)^{\gamma-1} \tag{4}$$

Since the solar wind is not homogeneous, the normalization constants $v_{\|0}$ and ρ_0 may vary from flux tube to flux tube, corresponding to different temperature and density at some arbitrary (coronal) reference level R_0. If we further assume that

$$\rho = \rho_0(R/R_0)^{-2} \tag{5}$$

which seems reasonable according to Figure 3, we finally obtain a relation between δ and γ by

$$\delta = (1-\gamma) + \ln (v_{\|0}^{(1)}/v_{\|0}^{(2)})/\ln (R_1/R_2) \tag{6}$$

If the reference thermal speeds at R_0 (in a structured corona, for example) varies within different flux tubes, the second term is nonzero. It vanishes only for a strictly homogeneous solar wind. This term could lead to a drastic overestimation of δ as compared to the $1-\gamma = -\frac{2}{3}$ adiabatic value. The worst case could be that for the two adjacent bins at $R_1 = 0.95$ and $R_2 = 0.85$ AU the reference value $v_{\|0}^{(1)}$ is largest and $v_{\|0}^{(2)}$ the lowest of our ensemble with average $\bar{v}_{\|0}$ and standard deviation $\Delta v_{\|0}$. Thus we may estimate the correction $\Delta\delta$ in (6) with $v_{\|0}^{(1)} = \bar{v}_{\|0} + \Delta v_{\|0}$ and $v_{\|0}^{(2)} = \bar{v}_{\|0} - \Delta v_{\|0}$ as

$$\Delta\delta = 9 \cdot 2 \cdot \Delta v_{\|0}/\bar{v}_{\|0} \tag{7}$$

For a relative fluctuation of a few percent in $v_{\|0}$ we obtain $\Delta\delta = O(1)$ for this worst case estimate. Since δ results from an average over many pairs of points and since also the case $v_{\|0}^{(1)} < v_{\|0}^{(2)}$ could occur, the actual $\Delta\delta$ is certainly smaller but still could be expected to give a large correction to $(1-\gamma)$.

This discussion may serve as a warning for the reader. One cannot readily infer from the comparatively flat average radial profile of $v_{\|,\perp}$ in Figure 4 that adiabaticity does not prevail. Two alternative, or even simultaneous, conclusions are then allowed. First, if one argues that $\Delta\delta$ is much smaller than 1, because the unknown $\Delta v_{\|0}/\bar{v}_{\|0}$ may be very small, then the results of Figure 4 indicate that the true polytropic index $\tilde{\gamma}$ must be smaller than $\frac{5}{3}$. This would imply another interplanetary source of thermal energy, denoted by the energy flux density Q_{WT}, which, for example, could be associated with waves and turbulence. We would than argue that this source is missing in the definition of γ in (1) and thus we should use instead

$$1/(\tilde{\gamma}-1) = 1/(\gamma-1) + (v_{WT}/v_\|)^2 \tag{8}$$

where $v_{WT} = (Q_{WT}/\rho u_r)^{1/2}$ is the typical equivalent speed related to Q_{WT}. The definition (8) follows from the discussion of polytropic models in *Parker*'s [1963] book. The $\tilde{\gamma}$ from Figure 4 is about $\frac{4}{3}$; thus we must have $(v_{WT}/v_\|)^2 \approx \frac{3}{2}$ in order to account for the required heating. If we take the velocity fluctuations δv associated with Alfvén waves, after *Feldman et al.* [1977] we have $v_{WT}^2 = \langle \delta v^2 \rangle = (35 \text{ km s}^{-1})^2$ in high-velocity streams at 1 AU. This number is somewhat smaller than our $v_\|$ at 0.95 AU, given in Table 3. However, closer to the sun, particularly in perihelion at 0.3 AU, the Helios observations yield a ratio of the Alfvén wave energy flux to the total enthalpy flux to order 1 or even slightly larger (see *Denskat* [1982, Table 5] or *Denskat et al.* [1981]). Thus by this simple energy argument it becomes clear that Alfvén wave damping could provide enough internal energy in order to account for nonadiabatic temperature profiles. We do not want to belabor this point too much but refer for details to the theoretical review by *Hollweg* [1978]. We could diminish the uncertainty $\Delta\delta$, introduced into our analysis by sampling different flux tubes, by relying solely on Helios lineup data. This has been done by *Schwartz and Marsch* [1983] for a typical high-velocity stream. But even then one is forced to average data over many measurement cycles, and thus one introduces statistical errors due to small-scale fluctuations.

The opposite conclusion from our results would be to reject the possibility of heat sources other than owing to particle heat flux degradation. Then the apparent discrepancy between the γ in Figure 8 and the indirectly inferred $\tilde{\gamma}$ from Figure 4 must be entirely attributed to the uncertain $\Delta\delta$ given by the second term in (6) and estimated roughly by (7). We may then conclude that our estimates of $\Delta\delta$ are compatible with an adiabatic expansion, where all nonadiabaticity can be explained by data sampling effects. This would necessarily imply that the Alfvén waves propagate more or less undamped between 0.3 and 1 AU. This possibility cannot be ruled out, since the observed reduction in the Alfvén wave energy flux [*Denskat et al.*, 1981] can within the experimental uncertainty entirely be explained by the expected natural decrease due to the work done by the Alfvén wave pressure on the expanding wind [*Belcher*, 1971].

We may reconcile these two extreme positions by admitting that both explanations are partly valid. Within experimental error and by fully realizing the serious limitations of our data analysis we cannot with certainty decide the question whether the solar wind, considered as a single fluid, expands adiabatically or not within the Helios orbital range between 0.3 and 1 AU.

APPENDIX

In this appendix we briefly summarize some mathematical equations and definitions of various parameters that have been analyzed experimentally by using the Helios data. For relevant references see the papers quoted in the introduction and the basic work by *Weber and Davis* [1967]. We shall adopt most of their formulas. However, we do not use a scalar pressure but the CGL pressure tensor instead and generalize the WD model insofar as we do not assume a polytropic equation of state but rather include the heat flux explicitly. Furthermore, since we allow for ion relative streaming, additional terms associated with the differential ion speed u_j appear in the total pressure and heat flux. All the other basic postulates of the WD model remain unaltered. Therefore the flow velocity and magnetic field vectors are only considered in the ecliptic plane, and it is assumed that their dependence on r is given by

$$\mathbf{u} = u_r(r)\mathbf{e}_r + u_\phi(r)\mathbf{e}_\phi \tag{A1}$$

$$\mathbf{B} = B_r(r)\mathbf{e}_r + B_\phi(r)\mathbf{e}_\phi \tag{A2}$$

Then the radial magnetic field component is determined from Gauss' law by

$$r^2 B_r = F_B \tag{A3}$$

The magnetic flux through an arbitrarily chosen reference sphere around the sun is one of the constants of motion and can readily be obtained from in situ measurements. The radial evolution of the magnetic field component B_ϕ is governed by Maxwell's equations and intimately related to the flow velocity via Ohm's law for the perfectly conducting solar wind plasma. In spherical coordinates one obtains from the curl of the electric field

$$r(u_r B_\phi - u_\phi B_r) = \text{const} = -\Omega r^2 B_r = -\Omega F_B \tag{A4}$$

Within WD's model the constant Ω can be consistently interpreted as the ordinary angular velocity of the sun at the photosphere, and thus (A4) yields no new constant of motion in addition to (A3). The equation of continuity implies the existence of another global constant of motion, which is the total mass loss rate of the sun per steradian,

$$r^2 \rho u_r = \dot{M} \tag{A5}$$

which, can be inferred from the Helios space probe plasma data between 0.3 and 1 AU. In spherical coordinates the balance of mechanical and magnetic stresses involves for the ϕ and r components of the tensor π

$$\frac{1}{r^3}\frac{d}{dr}(r^3 \pi_{\phi r}) = 0 \tag{A6}$$

Here the total stress tensor is defined by

$$\pi = \rho \mathbf{uu} + \mathsf{P} + (1/4\pi)(\tfrac{1}{2}B^2 \mathsf{1} - \mathbf{BB}) \tag{A7}$$

The thermal pressure is obtained by summing over the species intrinsic partial pressures (ρ_j is their mass density) and also contains the kinetic energy density associated with ion differential movement.

$$\mathsf{P} = \sum_j \rho_j [(v_{j\parallel}{}^2 + u_j{}^2)\mathbf{bb} + v_{j\perp}{}^2(\mathsf{1} - \mathbf{bb})] \tag{A8}$$

Here the species thermal speeds $v_{j\parallel,\perp} = (T_{j\parallel,\perp}/m_j)^{1/2}$ are expressed by the temperatures parallel and perpendicular to the magnetic field $\mathbf{B}(\mathbf{b} = \mathbf{B}/B)$, and u_j is the speed relative to the center of mass frame $\mathbf{u}_j = u_j \mathbf{b} = \mathbf{v}_j - \mathbf{u}$, where v_j is the species' main velocity. Note that the relative streaming enters in the total pressure exactly like the parallel thermal speed. With (A5), (A7), and (A8), equation (A6) can be cast into the form $\dot{M}L = \text{const}$, where the specific angular momentum per amu, L, is another constant of motion.

$$r\left\{u_\phi - \frac{B_r B_\phi}{4\pi\rho u_r}\left[1 - \frac{4\pi\rho}{B^2}(v_\parallel{}^2 - v_\perp{}^2)\right]\right\} = L \tag{A9}$$

The total angular momentum per unit mass comprises the particles' angular momentum, the magnetic torque, and thermal anisotropy torque, which in the solar wind plasma produces only a small correction [see *Weber*, 1970] to the isotropic angular momentum loss rate $\dot{M}L$ of the sun. We introduce the effective thermal speeds parallel

$$v_\parallel{}^2 = \sum_j \hat{\rho}_j (v_{j\parallel}{}^2 + u_j{}^2) \tag{A10a}$$

and perpendicular

$$v_\perp{}^2 = \sum_j \hat{\rho}_j v_{j\perp}{}^2 \tag{A10b}$$

to the magnetic field and $\hat{\rho}_j = \rho_j/\rho$, which is the fractional mass density of the species j.

Finally, as an equation for the radial flow velocity component u_r it is not advantageous to use directly the radial momentum equation. We may use instead the energy equation with the total energy flux density (Tr denotes the trace of a tensor)

$$\mathbf{S} = \tfrac{1}{2}\rho \mathbf{u}u^2 + \tfrac{1}{2}\,\mathrm{Tr}\,\mathsf{P}\mathbf{u} + \mathsf{P}\cdot\mathbf{u} + \mathbf{Q} + \frac{c}{4\pi}\mathbf{E}\times\mathbf{B} - \rho\mathbf{u}\frac{GM_S}{r} \tag{A11}$$

The total heat flux vector is given by $\mathbf{Q} = \frac{1}{2}(Q_\parallel + 2Q_\perp)\mathbf{b}$. Here $Q_{\parallel,\perp}$ refers to the center of mass frame and thus comprises intrinsic heat fluxes $q_{j\parallel,\perp}$ and enthalpy fluxes related to the species relative motion. One obtains

$$Q_\parallel = \sum_j (q_{j\parallel} + 3\rho_j u_j v_{j\parallel}{}^2 + \rho_j u_j{}^3) \tag{A12}$$

$$Q_\perp = \sum_j (q_{j\perp} + \rho_j u_j v_{j\perp}{}^2) \tag{A13}$$

for the multicomponent plasma. Note that also the species relative motion contributes to the total heat flux. The divergence of the total energy flux density reads in spherical coordinates

$$\frac{1}{r^2}\frac{d}{dr}(r^2 S_r) = 0 \tag{A14}$$

and thus yields another constant of motion, $\dot{M}\varepsilon$, where $\varepsilon = S_r/\rho u_r$. This is the energy flux divided by the mass flux or the energy per amu. This quantity is the most important one if one is interested in the evolution of the flow speed, since ε is a streamline constant and at 1 AU one finds $u_{1\,\mathrm{AU}} \approx (2\varepsilon)^{1/2}$ in the highly supersonic flow. The meaning and importance of ε in modeling the solar wind has been emphasized and demonstrated by *Holzer and Leer* [1980]. For one radial lineup of Helios 1 and 2, ε has been analyzed in all its constituents by *Schwartz and Marsch* [1983]. Since ε is not affected by the actual divergence of the flux tube, it should be insensitive to effects of rapidly diverging flux tubes. Some algebraic manipulations give

$$\varepsilon = \tfrac{1}{2}u_r{}^2 + \tfrac{1}{2}u_\phi{}^2 + \frac{B_\phi{}^2}{4\pi\rho} - \frac{u_\phi}{u_r}\frac{B_\phi B_r}{4\pi\rho} + \frac{1}{2\rho}\,\mathrm{Tr}\,\mathsf{P} + \frac{1}{\rho u_r}\mathbf{e}_r\mathbf{u}:\mathsf{P} + \frac{Q_r}{\rho u_r} - G\frac{M_S}{r} \tag{A15}$$

Various terms in (A15) can be grouped together in order to define potentials in the following way. The "magneto-rotational" potential combines the terms associated with the azimuthal kinetic energy and the Poynting flux as

$$\phi_\Omega = \tfrac{1}{2}u_\phi{}^2 + \frac{B_\phi{}^2}{4\pi\rho} - \frac{u_\phi}{u_r}\frac{B_\phi B_r}{4\pi\rho} \tag{A16}$$

Within the WD model this potential solely depends on heliocentric distance and the Alfvén Mach number and is proportional to L.

The "gravitational potential" can be written as

$$\Phi_G = -\tfrac{1}{2}v_\infty{}^2\left(\frac{R_S}{r}\right) \tag{A17}$$

where v_∞ denotes the escape speed from the solar surface to infinity. Note that $v_\infty = 618$ km s^{-1} is a large number com-

parable to typical solar wind speeds at 1 AU in recurrent high-velocity streams.

Finally, we define a "thermal potential" Φ_T comprising the pressure and heat flux terms in (A15). The quantity Φ_T attains the form

$$\Phi_T = \tfrac{1}{2}(v_\parallel{}^2 + 4v_\perp{}^2) + (v_\parallel{}^2 - v_\perp{}^2)\left(\frac{B_r}{B}\right)^2\left(1 + \frac{B_\phi}{B_r}\frac{u_\phi}{u_r}\right) + \tfrac{1}{2}(Q_\parallel + 2Q_\perp)\frac{B_r}{\rho u_r B} \quad \text{(A18)}$$

We introduce the following notation for the normalized heat fluxes

$$\alpha_{\parallel,\perp} = Q_{\parallel,\perp}B_r/(\rho u_r B v_{\parallel,\perp}{}^2) \quad \text{(A19)}$$

and the total pressure ratio or ratio of the squared thermal speeds by

$$A = (v_\perp{}^2/v_\parallel{}^2) \quad \text{(A20)}$$

Furthermore, it is convenient to define an "effective" polytropic index γ by

$$2/(\gamma - 1) = 1 + \alpha_\parallel + 2A(1 + \alpha_\perp) \quad \text{(A21)}$$

Then ϕ_T may also be rewritten with the help of (A4) as

$$\Phi_T = v_\parallel{}^2\left(\frac{\gamma}{\gamma - 1} + (1 - A)\frac{\Omega r}{u_r}\frac{B_\phi}{B_r}\Big/\left(1 + \left(\frac{B_\phi}{B_r}\right)^2\right)\right) \quad \text{(A22)}$$

This equation allows us to consider various interesting limits and a detailed comparison with data and previous theoretical models where a local equation of state was assumed to exist. Clearly, by definition, γ and the anisotropy A depend on r. If we restrict ourselves to the case $A = 1$ and constant γ corresponding to constant $\alpha_{\parallel,\perp}$ profiles, we regain the polytropic thermal potential, whereby $v_\parallel{}^2/\rho^{\gamma-1} = \text{const}$. We can now write the equation for the radial velocity component of the solar wind bulk flow in the compact form of (2).

Given a thermal potential Φ_T, equations (A3), (A4), (A5), (A9), and (2) provide a complete set of equations in order to determine the vectors in (A1) and (A2) and the density ρ. This will not be done in the present paper. Instead, we provide observational constraints on $\dot{M}$, L, ε, and F_B, which may serve as integration constants in solar wind models. A final comment concerns the solar wind linear momentum flux, which is found to be conserved by *Steinitz and Eyni* [1980]. Apparently, this cannot be strictly true for all radial distances, because the expanding solar wind has continuously to do work against solar gravity. However, if we have $u_r \gg v_A, u_\phi, v_{\parallel,\perp}$ and u_r larger than the local escape velocity from the sun's gravitational field (all of which is usually true between 0.3 and 1 AU), then the radial component of the momentum equation is simply given by

$$\frac{1}{r^2}\frac{d}{dr}(r^2\rho u_r{}^2) = 0 \quad \text{(A23)}$$

Thus the solar wind linear momentum flux is conserved. Since u_r itself is fairly constant beyond 0.3 AU, conservation of the mass flux implies $u_r\dot{M} = \text{const}$, and therefore (A23) is fulfilled. Our results presented in Figure 3 implicitly contain conservation of $r^2\rho u_r{}^2$. Explicit numbers for an even larger Helios data set can be obtained from *Schwenn* [1983]. In the present study we did not consider the linear momentum, since it is not a global constant of radial motion of the solar wind. What remains a puzzle, however, is that like $\varepsilon + \frac{1}{2}v_\infty{}^2$ also $u_r\dot{M}$ is found to be independent of the stream structure [*Steinitz and Eyni*, 1980; *Schwenn*, 1983].

Acknowledgments. The authors wish to thank R. Schwenn and H. Rosenbauer for reading of and comments on the manuscript. We also thank W. Pilipp for providing the electron data and F. M. Neubauer for making the magnetic field data available for this study. The Helios plasma experiment and its data evaluation are supported by the German Bundesministerium für Forschung und Technologie under grants WRS 10/7 and WRS 0108.

The Editor thanks E. Leer and another referee for their assistance in evaluating this paper.

REFERENCES

Acuna, M., and Y. C. Whang, A two-region model of solar wind including azimuthal velocity, *Astrophys. J.*, *203*, 720, 1976.

Asbridge, J. R., S. J. Bame, W. C. Feldman, and M. D. Montgomery, Helium and hydrogen velocity differences in the solar wind, *J. Geophys. Res.*, *81*, 2719, 1976.

Barnes, A., Acceleration of the solar wind by the interplanetary magnetic field, *Astrophys. J.*, *188*, 645, 1974.

Behannon, K. W., F. M. Neubauer, and H. Barnstorf, Fine-scale characteristics of interplanetary sector boundaries, *J. Geophys. Res.*, *86*, 3273, 1981.

Belcher, J. W., Alfvénic wave pressure and the solar wind, *Astrophys. J.*, *168*, 509, 1971.

Borrini, G., J. T. Gosling, S. J. Bame, W. C. Feldman, and J. M. Wilcox, Solar wind helium and hydrogen structure near the heliospheric current sheet: A signal of coronal streamers at 1 AU, *J. Geophys. Res.*, *86*, 4565, 1981.

Denskat, K. U., Untersuchungen von Alfvénischen Fluktuationen im Sonnenwind zwischen 0.29 AU and 1.0 AU, Dissertation, Tech. Univ. Braunschweig, F.R. G., 1982.

Denskat, K. U., F. M. Neubauer, and R. Schwenn, Properties of Alfvénic Fluctuations near the sun: Helios-1 and Helios-2, Solar Wind 4, *Rep. MPAE-W-100-81-31*, Max-Planck-Inst. für Aeron., Katlenburg-Lindau, F.R. G., 1982.

Feldman, W. C., J. R. Asbridge, S. J. Bame, M. D. Montgomery, On the origin of the solar wind proton thermal anisotropy, *J. Geophys. Res.*, *78*, 6451, 1973.

Feldman, W. C., J. R. Asbridge, S. J. Bame, M. D. Montgomery, and S. P. Gary, Solar wind electrons, *J. Geophys. Res.*, *80*, 4181, 1975.

Feldman, W. C., J. R. Asbridge, S. J. Bame, and J. T. Gosling, High-speed solar wind flow parameters at 1 AU, *J. Geophys. Res.*, *81*, 5054, 1976.

Feldman, W. C., J. R. Asbridge, S. J. Bame, and J. T. Gosling, Plasma and magnetic fields from the sun, in *The Solar Output and its Variations*, edited by O. R. White, Colorado University Press, Boulder, Colo., 1977.

Gosling, J. T., E. Hildner, J. R. Asbridge, S. J. Bame, and W. C. Feldman, Noncompressive density enhancements in the solar wind, *J. Geophys. Res.*, *82*, 5005, 1977.

Hollweg, J. V., Alfvén waves in the solar wind: Wave pressure, Poynting flux, and angular momentum, *J. Geophys. Res.*, *78*, 3643, 1973.

Hollweg, J. V., Collisionless heat conduction in the solar wind, *J. Geophys. Res.*, *81*, 1649, 1976.

Hollweg, J. V., Some physical processes in the solar wind, *Rev. Geophys. Space Phys.*, *16*, 689, 1978.

Holzer, T. E., and W. I. Axford, The theory of stellar winds and related flows, *Annu. Rev. Astron. Astrophys.*, *8*, 31, 1970.

Holzer, T. E., and E. Leer, Conductive solar wind models in rapidly diverging flow geometries, *J. Geophys. Res.*, *85*, 4665, 1980.

Hundhausen, A. J., Solar activity and the solar wind, *Rev. Geophys. Space Phys.*, *17*, 2034, 1979.

Leer, E., and T. E. Holzer, Constraints on the solar coronal temperature in regions of open magnetic field, *Solar Phys.*, *63*, 143, 1979.

Leer, E., T. E., Holzer, and T. Flå, Acceleration of the solar wind, *Space Sci. Rev.*, *33*, 161, 1982.

Lemons, D. S., and W. C. Feldman, Collisional modification to the exospheric theory of solar wind halo electron pitch angle distributions, *J. Geophys. Res.*, *88*, 6881, 1983.

Marsch, E., and H. Goldstein, The effects of Coulomb collisions on solar wind ion velocity distributions, *J. Geophys. Res.*, *88*, 9933, 1983.

Marsch, E., and A. K. Richter, Distribution of solar wind angular

momentum between particles and magnetic field: Inferences about the Alfvén critical point from Helios observations, *J. Geophys. Res.*, *89*, 5386, 1984.

Marsch, E., K.-H. Mühlhäuser, H. Rosenbauer, R. Schwenn, and F. M. Neubauer, Solar wind helium ions: Observations of the Helios solar probes between 0.3 and 1 AU, *J. Geophys. Res.*, *87*, 35, 1982*a*.

Marsch, E., K.-H. Mühlhäuser, R. Schwenn, H. Rosenbauer, W. Pilipp, and F. M. Neubauer, Solar wind protons: Three-dimensional velocity distributions and derived plasma parameters measured between 0.3 and 1 AU, *J. Geophys. Res.*, *87*, 52, 1982*b*.

Marsch, E., K.-H. Mühlhäuser, H. Rosenbauer, S. Schwenn, On the equation of state of solar wind ions derived from Helios measurements, *J. Geophys. Res.*, *88*, 2982, 1983.

Meyer, F., and D. Pfirsch, Korotation und Druckanisotropien im Sonnenwind, *Kleinheubacher Ber.*, *13*, 243, 1968.

Musmann, G., F. M. Neubauer, and E. Lammers, Radial variations in the interplanetary magnetic field between 0.3 and 1.0 AU, *J. Geophys.*, *42*, 591, 1977.

Neubauer, F. M., G. Musmann, and G. Dehmel, Fast magnetic fluctutions in the solar wind: Helios 1, *J. Geophys. Res.*, *82*, 3201, 1977*a*.

Neubauer, F. M., H. J. Beinroth, H. Barnstorf, and G. Dehmel, Initial results from the Helios-1 search-coil magnetometer experiment, *J. Geophys. 42*, 599, 1977*b*.

Neugebauer, M., Observations of solar wind helium, *Fundam. Cosmic. Phys.*, *7*, 131, 1981.

Neugebauer, M., Observational constraints on solar wind acceleration mechanisms, Solar Wind 5, *NASA Conf. Publ., CP-2280*, 1983.

Ogilvie, K. W., and J. D. Scudder, The radial gradients and collisional properties of solar wind electrons, *J. Geophys. Res.*, *83*, 1524, 1978.

Olbert, S., Inferences about the solar wind dynamics from observed distributions of electrons and ions, Proceedings of an International School and Workshop on Plasma Astrophysics, Varenna (Como), Italy, *ESA SP-161*, p. 135, Eur. Space Agency, Neuilly, 1981.

Parker, E. N., *Interplanetary Dynamical Processes*, Interscience, New York, 1963.

Pilipp, W. G., Solar-wind electrons as a probe for the global structure of the interplanetary magnetic field, in *Topics in Plasma, Astro and Space Physics*, edited by G. Haerendel and B. Battrick, p. 91, Max-Planck-Institut für Extraterrestrische Physik, Garching/Munich, F.R.G., 1983.

Pilipp, W. G., R. Schwenn, E. Marsch, K.-H. Mühlhäuser, and H. Rosenbauer, Solar Wind 4, *Rep. MPAE-W-81-31*, Max-Planck-Inst. für Aeron., Katlenburg-Lindau, F. R. G., 1981.

Pizzo, V., R. Schwenn, E. Marsch, H. Rosenbauer, K. H. Mühlhäuser, and F. M. Neubauer, Determination of the solar wind angular momentum flux from Helios data—An observational test of the Weber and Davis theory, *Astrophys. J.*, *271*, 335, 1983.

Rosenbauer, H., H. Miggenrieder, M. D. Montgomery, and R. Schwenn, Preliminary results of the Helios plasma measurements, in *Physics of Solar-Planetary Environments: Proceedings of the International Symposium on Solar-Terrestrial Physics*, edited by D. J. Williams, p. 319, AGU, Washington, D. C., 1976.

Rosenbauer, H., R. Schwenn, E. Marsch, B. Meyer, H. Miggenrider, M. D. Montgomery, K.-H. Mühlhäuser, W. Pilipp, W. Voges, and S. M. Zink, A survey of initial results of the Helios plasma experiment, *J. Geophys.*, *42*, 561, 1977.

Schwartz, S. J., Plasma instabilities in the solar wind: A theoretical review, *Rev. Geophys. Space Phys.*, *18*, 313, 1980.

Schwartz, S. J., and E. Marsch, The radial evolution of a single solar wind plasma parcel, *J. Geophys. Res.*, *88*, 9919, 1983.

Schwenn, R., The "average" solar wind in the inner heliosphere: Structures and slow variations, Solar Wind 5, *NASA Conf. Publ., CP-2280*, 489, 1983.

Schwenn, R., H. Rosenbauer, H. Miggenrieder, Das Plasmaexperiment auf Helios (E1), *Raumfahrtforschung*, *19*, 226, 1975.

Schwenn, R., M. D. Montgomery, H. Rosenbauer, H. Miggenrieder, K.-H. Mühlhäuser, S. J. Bame, W. C. Feldman, and R. T. Hansen, Direct observation of the latitudinal extent of a high-speed stream in the solar wind, *J. Geophys. Res.*, *83*, 1011, 1978.

Spitzer, L., *Physics of Fully Ionized Gases*, Interscience, New York, 1962.

Steinitz, R., and M. Eyni, Global properties of the solar wind, I, The invariance of the momentum flux density, *Astrophys. J.*, *241*, 417, 1980.

Weber, E. J., The torque on the interplanetary plasma due to its anisotropy, *Solar Phys.*, *13*, 240, 1970.

Weber, E. J., and L. Davis, The angular momentum of the solar wind, *Astrophys. J.*, *148*, 217, 1967.

Weber, E. J., and L. Davis, The effects of viscosity and anisotropy in the pressure on the azimuthal motion of the solar wind, *J. Geophys. Res.*, *75*, 2419, 1970.

E. Marsch and A. K. Richter, Max-Planck-Institut für Aeronomie, Postfach 20, D-3411. Katlenburg-Lindau, F.R.G.

(Received November 1, 1983;
revised February 27, 1984;
accepted April 17, 1984.)